

Review

# The Trends of TiZr Alloy Research as a Viable Alternative for Ti and Ti16 Zr Roxolid Dental Implants

Daniela Ionita <sup>1</sup>, Cristian Pirvu <sup>1</sup>, Andrei Bogdan Stoian <sup>1</sup> and Ioana Demetrescu <sup>1,2,\*</sup>

<sup>1</sup> Department of General Chemistry, University Politehnica of Bucharest, 313 Splaiul Independentei, 060042 Bucharest, Romania; daniela.ionita@upb.ro (D.I.); cristian.pirvu@upb.ro (C.P.); andreibstoian@yahoo.com (A.B.S.)

<sup>2</sup> Romanian Academy of Scientists, 54 Splaiul Independentei, 50085 Bucharest, Romania

\* Correspondence: i\_demetrescu@chim.upb.ro; Tel.: +40-214-023-930

Received: 25 March 2020; Accepted: 20 April 2020; Published: 24 April 2020



**Abstract:** Despite many discussions about Ti versus Zr, Ti remains the golden standard for dental implants. With the extended use of implants, their rejection in peri-implantitis due to material properties is going to be an important part of oral health problems. Extended use of implants leading to a statistical increase in implant rejection associated with peri-implantitis raises concerns in selecting better implant materials. In this context, starting in the last decade, investigation and use of TiZr alloys as alternatives for Ti in oral dentistry became increasingly more viable. Based on existing new results for Ti16Zr (Roxolid) implants and Ti50Zr alloy behaviour in oral environments, this paper presents the trends of research concerning the electrochemical stability, mechanical, and biological properties of this alloy with treated and untreated surfaces. The surface treatments were mostly performed by anodizing the alloy in various conditions as a non-sophisticated and cheap procedure, leading to nanostructures such as nanopores and nanotubes. The drug loading and release from nanostructured Ti50Zr as an important perspective in oral implant applications is discussed and promoted as well.

**Keywords:** Ti16Zr; Ti50Zr; anodizing; electrochemical stability; mechanical properties; drug loading

## 1. Introduction

The advancement of science and technology has led to a constant improvement of dental implants. The studies performed on stainless steels, cobalt-chromium, titanium alloys, and zirconia have provided suitable data to conveniently select materials appropriate for restoration works and implants in dentistry [1–3].

The extended use of dental implants is leading to a statistical increase of the number of patients that suffer inflammatory processes of the tissues surrounding implants and eventual rejection of the implants [4]. This inflammatory process is a result of bacterial biofilm accumulation as a function of diseases such as peri-implantitis, which is a chronic pathological microbial process [4] that affects the soft tissue and surrounding bone areas of an implant.

Implant loss can be attributed to a number of factors, ranging from the bone quality and general health of the patient [5] to the incompatibility of the implant, in addition to incorrect insertion techniques. Implant rejection in peri-implantitis caused by the materials' properties and their behavior [6] is an important part of oral health problems. Based on ratios between cortical and trabecular tissues, as well as vascularization, bones can be classified into four types, with type I being the most dense and least vascularized, and type IV being the lightest but with high vascularization. One finite element study [5]

established functional loads and how bone loss affects the longevity of the implants. This study found that implants have a lifetime of more than 10 years in type I bones, and strains were immediately deleterious for implants in type IV bone. Material properties, incorrect insertion techniques, and the incompatibility of the implant are other factors of implant rejection [6].

In this context, selection of dental implant materials and procedures for their improvements need more attention, and research in the field of biomaterials is a new dynamic challenge.

Titanium (Ti) has merits such as high resistance to corrosion and biocompatibility. Ti has a silvery grey-white color that darkens when oxides are formed on its surface. Ti alloying was chosen mostly to improve different properties, and a large variety of such alloys were proposed and investigated [7,8]. The introduction of alloying elements changes the phase compositions of Ti ( $\alpha$ ,  $\beta$ , and  $\alpha$ - $\beta$ ), modifying the bulk Ti-alloy properties as well [9]. The  $\alpha$  alloys have a hexagonal closely packed crystallographic structure, while the  $\beta$  alloys have a body-centered cubic form. Ti is an  $\alpha$ -type material, having a closely packed hexagonal structure and a density of  $4.5 \text{ g/cm}^3$ . The  $\alpha$  to  $\beta$  transformation temperature of Ti changes from  $882 \text{ }^\circ\text{C}$  to a higher temperature with an  $\alpha$  stabilizer such as Al, or to a lower value with a  $\beta$  stabilizer such as V. In the case of Ti6Al4V, which is the most common ternary Ti alloy used in dentistry, the  $\alpha$ -phase is stabilized by Al, which increases the strength of the alloy but also, due to its low density ( $2.7 \text{ g/cm}^3$ ) lowers the density of the alloy. The  $\beta$ -phase is stabilized by V, which enhances the ultimate tensile strength, lowering the elongation [10]. The  $\beta$  alloys are more advantageous in processing compared to  $\alpha + \beta$  alloys, because of their lower modulus of elasticity, which is closer to that of bone [8].

Ti forms spontaneously on its surface oxide particles ( $\text{Ti}_x\text{O}_y$ ), which cover the surface of the metal with a film of around 3–10 nm in thickness, which is very stable and has high corrosion resistance. The Ti oxide layer can adsorb Ca and P ions, forming apatite. It can also adsorb some proteins, promoting osseointegration, depending on surface characteristics such as micro- and nanoroughness [11]. Ti6Al4V has standard specifications and is largely used for orthopaedic and dental implants due to its mechanical aspects, such as high strength and fatigue performance [12]. The release of V and Al ions resulting from corrosion has been shown to cause detrimental health effects [13]. Ti6Al7Nb, a substitute for Ti6Al4V, has gained more interest for surgical implants [14]. This alloy still incorporates Al, a potentially dangerous element in the human body that is able to induce osteoporosis and some degenerative diseases [15]. Such aspects related to ternary alloys prompted researchers to study binary alloys, and according to literature [9], the binary Ti alloys with Zr, In, Ag, Cu, Au, Pd, Nb, Mn, Cr, Mo, Sn, and Co have potential as implant materials based on their mechanical performance and favorable biological behaviour.

Zr has a higher density than Ti ( $6.52 \text{ g/cm}^3$ ), a convenient Young's modulus at 88 GPa, and a lateral shear strength of 33 GPa. Zr spontaneously produces a native passive oxide film on the surface named "zirconia" ( $\text{ZrO}_2$ ), has better osseointegration when compared to Ti [16,17], and is not affected by plaque accumulation in the oral cavity. In the last decade, alloys of Zr and Ti in different proportions were more intensely investigated as alternatives for Ti in applications of restorative works [18,19], having better mechanical properties than Ti and having excellent in vitro and in vivo behaviour [17,18]. Both Ti and Zr are excellent for use in dental implants, but the advantage of TiZr alloying is the increased mechanical stability [20] compared to cp-Ti, having an endurance level 13%–42% higher compared to cp-Ti implants with the same dimensions. In 2009, Straumann introduced Roxolid (Ti 13%–17% Zr) as a small dimensional implant (3.3 mm in diameter) that could be used in molar and premolar restorations, eliminating the need for additional bone structure [21]. Roxolid is a representative metallic biomaterial for implants, especially for cases where the space between teeth is limited. Values for different mechanical properties of materials used as implants are shown in Table 1.

**Table 1.** Mechanical properties of Ti and Ti-based alloys (adapted from [8,16,18,20]).

| Material       | Young's Modulus (GPa) | Tensile Strength (MPa) | Elongation (%) | Density (g/cm <sup>3</sup> ) |
|----------------|-----------------------|------------------------|----------------|------------------------------|
| cp-Ti          | 104                   | 450                    | 15             | 4.5                          |
| Ti6Al4V        | 113                   | 860                    | 10             | 4.4                          |
| Ti6Al7Nb       | 100                   | 995                    | 14             | 4.5                          |
| Roxolid Ti16Zr | 54.5                  | 953                    | 12             | 4.75                         |

A series of TiZr alloys were compared with cp-Ti. The Ti<sub>x</sub>Zr alloys with Zr content ranging from 5% to 85% were characterized [22–24] in terms of stress distribution, surface topography at the micro-level, electrochemical stability in a simulated oral cavity environment, in vitro cell cultures, and pre-clinical and clinical studies. Fracture of the implant body and bone resorption caused by stress around implants were investigated by finite element method, and clinical investigations concluded that the narrow-diameter TiZr implants present similar success rates and peri-implant bone resorption as cp-Ti implants of comparable dimensions [24].

The corrosion investigations revealed from the polarization curves that the alloys with Zr contents [25] ranging between 10% and 50% had a large passive range (an inactive state of metals in Pourbaix equilibrium diagrams), which increased with the Zr amount, and were resistant to localized corrosion. Recently, it was shown that the degradation of the oxide layer formed on alloys with more than 50% Zr led to the apparition of local corrosion [26]. The results from the electrochemical studies, coupled with the superior mechanical behaviour of Ti50Zr [27], make this alloy suitable as another candidate for safe dental implants [28–31], which needs more consideration regarding its use as an alternative for Roxolid in dentistry.

In addition to their excellent biocompatibility and electrochemical stability, which make them perfectly suited for biomedical applications, Ti and Zr have uses in other fields of science, including as catalysts for reactions [32,33], photocatalysts [34], or dye-sensitized solar cells [35].

The goal of this manuscript is to illustrate the merits of Ti50Zr in oral cavities as functions of surface treatment. Based on the existing expertise, we chose to present the unmodified and modified surface properties of Ti50Zr [36–38] with better biocompatible antibacterial coatings. Drug loading and release from such coatings [39–42] are discussed as a part of the coated Ti50Zr performance, and future trends in dental materials applications are presented.

## 2. Ti<sub>x</sub>Zr Alloys

Structural investigation indicated that  $\alpha$  and  $\alpha'$  phases exist in Ti<sub>x</sub>Zr alloys. The X-ray diffraction patterns of alloys revealed that the  $\alpha$  phase corresponds to a structure rich in Ti and the  $\alpha'$  phase to a Zr-rich structure. The porosity of Ti<sub>x</sub>Zr alloys was about 10% [20]. The Zr content in the studied alloys ranged from 5% to 45%. The alloys exhibited a decrease of the elastic modulus (from 59 GPa to 53 GPa) with the increase of Zr content, which remained lower than that of Ti (104 GPa). One reason for the decrease of the modulus is probably the occurrence of pores in the alloy. Another reason may be the increase of interatomic distance after Zr addition, leading to an interatomic force decrease.

Electrochemical results for Ti<sub>x</sub>Zr performed in many tested solutions, such as physiological solution (NaCl 0.9%), simulated body fluid, and Fusayama saliva, indicate a better stability than Ti and an increase of corrosion resistance with Zr content in the alloy [43,44]. The fact that TiZr alloys exhibit superior electrochemical behaviors than cp-Ti is attributed to their more resistant passive layer containing Ti<sub>2</sub>O<sub>3</sub>, TiO<sub>2</sub>, and ZrO<sub>2</sub> [45]. A test of a dental implant performed with 1000 h of immersion in Carter–Brugirard saliva with pH values that simulate the conditions in the oral cavity showed how the protective properties of Ti20Zr were enhanced due to the new phosphate-rich layer that formed at the interface [45]. Other papers [46] focus on the detection of the cause of the Ti6Al4V dental implant's fracture during the cutting process on the basis of its structural and fractographic analysis. Recently, a study of the corrosion resistance of TiZr binary alloys evidenced an interesting finding when

correlating the electrochemical results with the composition change. The samples were cp-Ti, Ti10Zr, Ti30Zr, Ti50Zr, Ti70Zr, and pure Zr. The corrosion resistance was evaluated by anodic polarization using Fusayama artificial saliva and a solution of lactic acid with added NaCl [26]. The aim of this study was to promote corrosion of the whole alloy components, with Zr being corroded by chloride ions, whereas Ti was corroded by the lactic acid + NaCl mixture. Based on literature results, Figure 1 presents the corrosion current density dependence as a function of Zr content for different  $Ti_xZr$  alloys.

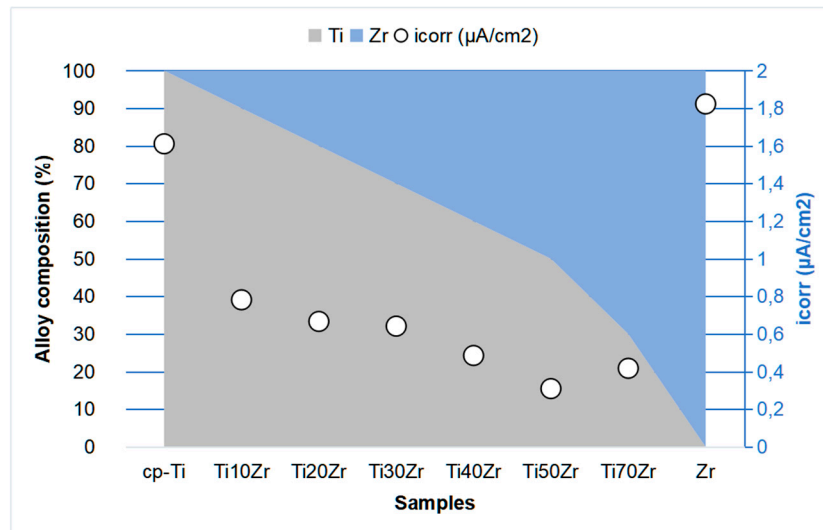


**Figure 1.** Corrosion density current dependence of  $Ti_xZr$  alloy as a function of Zr content.

The content limit with a positive effect is 50% Zr. The degradation of the oxide layer, which led to the development of local corrosion, was observed in alloys with less than 30% and with more than 50% Zr content, which led to the development of local corrosion. We can assume that in the case of  $TiZr$  alloys, a percentage of less than 30% of any element has a negligible effect and that the alloy behaves as the dominant metal.

Ti50Zr maintains its good stability in aggressive media; however, the same material can have slightly different behaviors in various electrolytes, as exemplified in Figure 2.

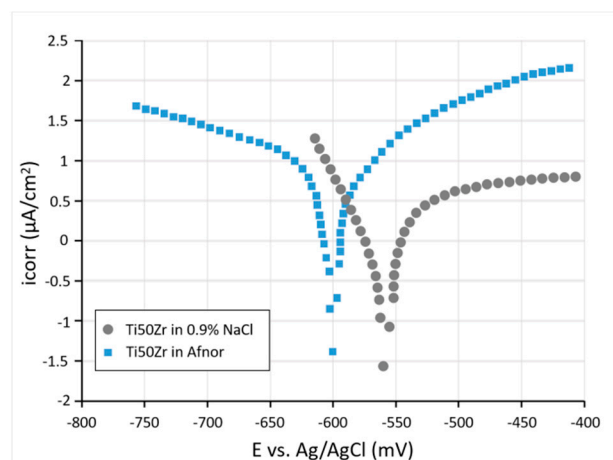


**Figure 2.** Tafel plots for Ti50Zr resulting from measurements in NaCl 0.9% and Afnor artificial solution.

The observed superior electrochemical and mechanical properties of Ti50Zr [27] suggest that this material can safely replace Roxolid as a dental implant. It is known that despite the use of a good

method of implantation and a suitable treatment after this operation, bone loss can still occur [46,47]. The fracture of the central screw and other implant parts was investigated and the results showed that implant failure is mainly caused by mechanical aspects [48,49], such as fatigue or overload with high-level cyclic stresses. In artificial saliva, the passive film of the implant is damaged under cyclic tensile loading. Local corrosion takes place when the film is destroyed and can further develop into fatigue as an expression of a corrosion-assisted fatigue process. In a recent mechanical test [27], according to ISO 14801 standard [50], the commercial Roxolid Ti16Zr alloy was compared to Ti50Zr. The experimental results show that Ti50Zr limits were up to  $1001 \pm 8$  MPa for strength and up to  $500 \pm 10$  MPa for fatigue, representing an improvement of between 23% and 32%. The maximum cycling loads for Ti50Zr implants were 400 N in air, 400 N in artificial saliva, and 350 N for sandblasted, large grit, acid-etched implant surfaces (SLA) ( $5 \times 10^6$  cycles without failure). Such improvement of the mechanical properties for Ti50Zr [27] is attributed to various factors, such as the mechanism of acicular martensite strengthening, presence of nanotwins, and dislocation strengthening.

### 3. Ti50Zr Alloy Surface Modification

The biological effects of a biomaterial are largely determined either independently or associatively through its corrosion resistance, composition (surface chemistry), topography, microroughness, and surface energy [51].

As was highlighted above, the corrosion resistance is a key parameter in establishing the suitability of a metal for use in surgical implants. The corrosion resistance of Ti and Ti alloys comes from their tremendous affinity for oxygen and due to their spontaneous tendency to form a natural protective oxide layer when the metal is exposed to the atmospheric environment. Due to the high surface energy, Ti and its alloys are very reactive metals, which in air form a compact and thin oxide film adherent on the substrate in milliseconds, measuring approximately 1.5–10 nm in thickness [52,53]. TiZr shows the highest corrosion resistance in the presence of cells (cell assays using human lymphoid cells (CEM) and MC3T3-E1 cells) and various electrolytes compared with cp-Ti and Ti6Al4V alloys [18,54]. The evaluation of oral microbial corrosion of dental implant materials revealed that TiZr surfaces had similar behaviors regarding colonization and surface degradation by oral *Streptococcus* species to those of cp-Ti [55]. The oxides and hydroxides of Ti and Zr have low solubility, acting as passive oxide films with excellent corrosion resistance. The fact that the Ti alloy biomaterials are covered with oxides not only inhibits corrosion but also increases biocompatibility. Thus, there is a sustained concern for growing and organizing oxide layers on the surface of these alloys in order to improve the surface properties [55–63].

Oxidation of TiZr alloy in air or oxygen has been studied since 1994, highlighting the role of alloy composition in kinetic and morphological evolution from pure Ti to pure Zr [64,65].

Biomimetic TiZr foams with macropores and micropores were fabricated by mechanical alloying using amorphous TiZr alloy powder. The porous structure and the mechanical properties of the TiZr foam were very close to those of natural bone [66].

A good in vitro bioactivity was demonstrated after TiZr surface modification by alkali heat treatment, leading to the formation of a bioactive nanoporous sodium titanate/zirconate hydrogel surface layer. This surface modification induced the deposition of calcium phosphates during the immersion in simulated body fluid (SBF), making TiZr an attractive artificial bone material with a good equilibrium between bioactivity, excellent mechanical properties, and low processing costs [67]. It was discovered that the roughness of the surface is an important factor determining apatite formation on the surfaces. The island-like spherulites of apatite deposited on treated surfaces after being incubated in the SBF for 7 days showed that these particles preferred to cling to the surface along the grooves created during the grinding process [68]. An average roughness of approximately 600  $\mu\text{m}$  led to the forming of a dense, uniform, and continuous apatite layer for two weeks on Ti and three weeks on Zr and TiZr after immersion in SBF [69]. Sol-gel-derived HA/TiO<sub>2</sub> [70], hydroxyapatite-chitosan

composite [71] and biomimetic processed nanocrystallite apatite coatings [72] were also deposited on TiZr to improve the bone-like apatite deposition from SBF.

Self-organized and highly ordered oxide nanostructures were obtained by TiZr anodizing. A schematic representation is shown in Figure 3. The anodizing process involves the application of a suitable voltage to the surface of a metal and the formation of metal cations. Depending on the conditions, the metal cations that can either dissolve or react with existing  $O^{2-}$ , forming a metal oxide layer on the surface of metal. The metal oxide can be insoluble or be partially dissolved due to the composition and conditions of the electrolyte [73].

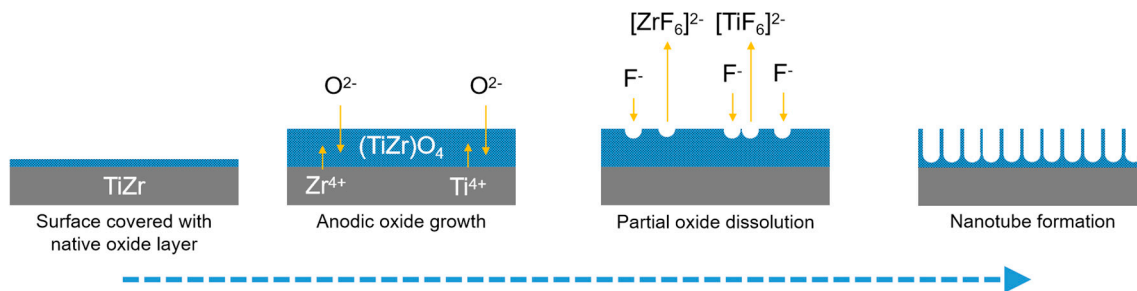


**Figure 3.** Schematic representation of the process for obtaining ordered TiZr oxide nanostructures.

The reported electrolytes can be divided into four categories: acidic, buffered, polar organic, and non-fluoride-based [74,75]. The nanotubular surface produced by anodization can promote accelerated attachment and differentiation of osteoblast cells, enhancing their behaviour at the cellular and molecular levels. Higher hydrophilicity and roughness attract more tissue fluid to increase the migration and arrangement of osteogenic cells, which is beneficial to osseointegration. Microvilli and filopodia are more easily permeable to the energy barrier between the material and the cells themselves at the early stage of cell attachment. Significant extension of the cell process was observed on anodized surfaces compared to non-anodized surfaces [75]. Thus, optimization of surface properties in terms of morphology, surface wettability, enlarged surface area, and microroughness can synergistically improve the biological behaviour of cells attached on the materials [76]. Since 2010, Schmuki has reported formation of the nanotube bundles (10–15 nm diameters) on TiZr by one-step anodization in chloride–perchlorate mixed solution buffered at pH = 4 [77]. Then,  $TiO_2$ – $ZrO_2$  nanotubes with different diameters (20–70 nm) were produced in two-step anodization procedures, applying different potentials in a range from 15 to 45V on Ti50Zr [78]. Two-step anodization procedures form nanotube coatings containing crystalline phases, both before and after annealing [38]. All nanotubular samples provided better cell viability than the base metal. Samples anodized at smaller potentials (5–10 V) formed only nanopores, with diameters increasing with the increase of the applied potential from 8 nm to 33 nm [23]. The larger diameters and hydrophilic character of samples anodized in two steps at 15 and at 30 V were correlated with higher rates of cell proliferation and viability. However, no detectable expression of mRNA for osteocalcin and osteonectin was observed [78]. Less proliferative cultures observed on nanotubes formed at 45 V manifested osteogenic differentiation [76]. The hydrophilic properties of the nanotubular surface of one-step anodized Ti50Zr increased with an increase in the  $F^-$  concentration and the applied potential due to changes in the distribution of the nanotube size. Generally, the water contact angle on these surfaces decreased when the roughness parameters and surface energy of the surface increased. The surface energy followed the same increasing trend of hydrophilic properties [73]. Surfaces with small-diameter nanotubes (20–30 nm) showed better antibacterial effects compared to those with larger diameters (50–70 nm), due to the smaller active area available for bacterial colonization on such nanotubes [79]. The mixed nanotubes composed of  $TiO_2$ – $ZrO_2$ – $ZrTiO_4$  formed on Ti50Zr with variable nanotube size, distribution, and other properties, such as surface wettability and microroughness, are more promising for biomedical applications

than the 100% TiO<sub>2</sub> nanotubes formed on cp-Ti [74,75]. Nevertheless, other studies state that the composition of the surface oxide layer is not important in determining osseointegration kinetics [80].

The fabrication of nanochannelar non-thickness-limited 1D structures by anodizing Ti50Zr in hot glycerol-phosphate electrolyte has been also reported [29]. The nanostructures were partially crystalline, composed of anatase, ZrO<sub>2</sub>, and orthorhombic srilankite. The surface morphology and chemistry produced higher hydrophilicity and improved corrosion resistance compared to compact oxide layers produced in the same alloy. In vitro studies performed on RAW 264.7 macrophages showed the potential of surfaces covered with nanochannels to reduce foreign body reactions against Ti50Zr biomedical implants. This phenomenon is achieved by decreasing the proliferation rate, supporting macrophage adhesion but not permitting macrophage fusion, thus reducing the inflammatory response. Ti50Zr surfaces covered with nanochannels improve the adhesion and proliferation of mouse pre-osteoblast MC3T3-E1 cells and enhance their osteogenic differentiation. This specific nanochannelar topography inhibits nuclear factor kappa-B ligand (RANKL)-mediated osteoclastogenesis. The TiZr surface modification with nanochannel structures could be a viable strategy for fabricating Ti alloy implants able to inhibit bone resorption and improve osseointegration [30].

Ti50Zr surfaces were coated with n-type semiconductor TiO<sub>2</sub> nanowires by electrospinning, improving the surface hydrophilicity and corrosion behaviour without generating significant inflammatory processes [39].

Sandblasted, large grit, acid-etched TiZr dental implant surfaces enhanced hydrophilicity significantly, promoting better adsorption of certain proteins and osteoblastic differentiation and maturation of human bone mesenchymal stem cells (hBMSCs) [80–83]. The mRNA levels of bone morphogenic proteins (BMPs) were increased. They are known to promote osteogenesis, which facilitates osteoblastic differentiation and maturation [83].

Plasma electrolytic oxidation treatment appears to be a feasible alternative for Ti15Zr surface modification with biofunctional coating, improving surface characteristics and electrochemical stability, as well as enhancing the adsorption of albumin on the material surface and limiting bacterial adhesion [81].

#### 4. Drug Loading and Release from Anodized Ti50Zr

A promising strategy for releasing drugs on the target site is to incorporate them in implants, thus achieving minimal systemic adverse effects. Ti and its alloys have good biocompatibility and ability to form a variety of nanostructures on their surfaces suited for controlled loading and release of drugs. The main advantages of these nanostructures is the relative ease of fabrication and the control of their characteristics (length, diameter, wall thickness, corrosion resistance, wettability, etc.) [84–87]. The main mechanisms for drug delivery are diffusion, erosion, and swelling, which can be tweaked by varying the characteristics of the nanostructures, or even controlled by applying electrical or magnetic fields, osmotic pressure, or drug convection along fluids.

The drug release from TiO<sub>2</sub> nanotubes is mainly based on desorption and diffusion. Fickian equations are usually employed to describe the diffusion and drug release kinetics from implants by estimating the concentration change with respect to time due to diffusion. Several other release models were developed (Equations (1)–(4)), namely Higuchi, Korsmeyer–Peppas, Peppas–Sahlin, and Lindner–Lippold models [88–91]. The equations used to illustrate the diffusion parameters are:

$$Y = kt^{0.5} \quad (1)$$

$$Y = kt^n \quad (2)$$

$$Y = at^n + bt^{2n} \quad (3)$$

$$Y = kt^n + b \quad (4)$$

where  $Y$  is the drug fraction released at time  $t$ ,  $k$  is a kinetic constant that incorporates the structural and geometric characteristics of the system, and  $n$  is the exponent that indicates the mechanism of release. The values of  $n$  depend on the geometry of the carrier; for cylinders, Fickian diffusion is represented with  $n \sim 0.5$ , anomalous transport with  $0.45 < n < 0.89$ , and relaxational case II transport with  $n > 0.89$ .

Drug release depends not only on nanotube surface chemistry, surface area, and pore size, but also on drug molecule size, charge, drug solubility, and diffusion coefficients.

A larger molecule experiences difficulties in the loading mechanism, rendering a greater portion of the drug as surface-bound instead of inside the nanostructures, producing an early-phase burst.

The Desai group fabricated different types of  $\text{TiO}_2$  nanotubes, varying their dimensions to better understand the release rates of albumin, lysozyme, and antibiotics (sirolimus and paclitaxel) [92,93]. They were able to control the release of these molecules through burst release, where the majority was eluted in a few hours, as well as through prolonged release over a week. Nemati and Haljizadih loaded gentamicin on simple and nanostructured Ti surfaces, observing that the drug was released in 30 min from the bare Ti surface and in 3 days from the anodized surfaces [94].

To achieve prolonged release of drugs, some studies proposed biodegradable films to seal the loaded nanostructures [95]. Gentamicin encapsulation in  $\text{TiO}_2$  nanotubes was studied by Kumeria et al. [96], who sealed the nanotubes with chitosan and PLGA. The observed release rates of gentamicin ranged from 7 days for the uncapped nanotubes to 22 days for chitosan encapsulation and 27 days for PLGA encapsulation. Our group studied nanoporous and nanotubular TiZr surfaces as drug delivery systems for gentamicin. The nanostructured surfaces were covered with pores ( $\sim 70$  nm in diameter and 100 nm in depth) or nanotubes ( $\sim 120$  nm interior diameters and lengths reaching  $10 \mu\text{m}$ ) by anodization. Gentamicin (molecular size  $< 1$  nm) was bound on these surfaces by physical adsorption. The loaded nanostructures were then coated with chitosan. Figure 4 shows a schematic representation of obtained coated nanostructures and drug release.

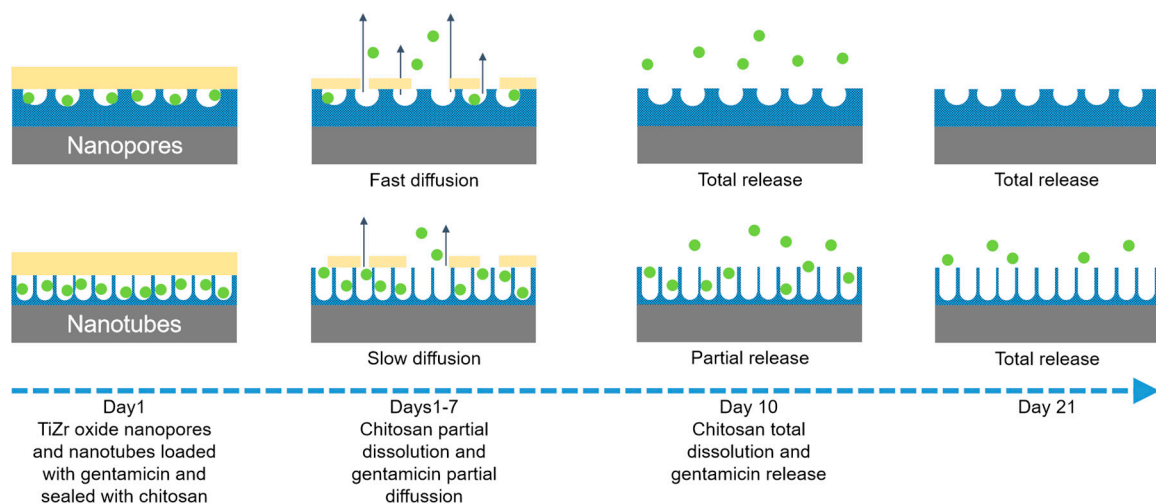


**Figure 4.** Schematic representation of the obtained coated nanostructures and drug release over time.

The gentamicin release mechanism was studied with three mathematical models: Korsmeyer–Peppas, Peppas–Sahlin, and Lindner–Lippold models. A faster release rate was observed in the case of nanopores, with 95% of the amount of gentamicin being released in 10 days from the nanoporous structures and in 21 days from nanotubes. The best approximation for the release mechanism was obtained with the Lindner–Lippold model [40].

A balance must be reached between short-term fast delivery of high doses, which can reach toxic levels, and long-term slow release, which may not reach the desired therapeutic level. The risk in slowly releasing antibiotic systems is that there strains of bacteria may survive the initial contact

with the drug, thus developing resistance. Ideally, the antibiotics should be introduced immediately post-surgery before the formation of the bacterial biofilm. It is known that the dose necessary to destroy bacteria-protected biofilms is about 1000 times higher than that necessary to neutralize bacteria in suspension. Therefore, the local release of antibiotics should be divided into two stages: a fast initial release lasting up to 6 h after intervention in order to aid the weakened immune system and a slow release lasting up to a few days as a prophylactic, combating the latent infection [97,98]. In our studies of gentamicin release from nanoporous and nanotubular TiZr oxide structures, the minimum effective gentamicin concentration against most bacteria (1–4 µg/mL) [40] was reached in 4 h after immersion.

Another suggested mechanism for gentamicin loading is presented in Figure 5. Gentamicin loading can occur either by physical deposition in the  $\text{TiO}_2\text{-ZrO}_2\text{-ZrTiO}_4$  nanotubes or due to the electrostatic interactions between the negative charges of nanotubes and positive charges of gentamicin in physiological pH (7.4). Gentamicin is an aminoglycoside antibiotic mixture of three major components, namely gentamicin C1 (R1 = R2 = CH<sub>3</sub>), C1a (R1 = R2 = H), and C2 (R1 = CH<sub>3</sub>; R2 = H), as well as a number of minor components. At pH = 7.4, aminoglycosides have a high positive charge and behave as cations.

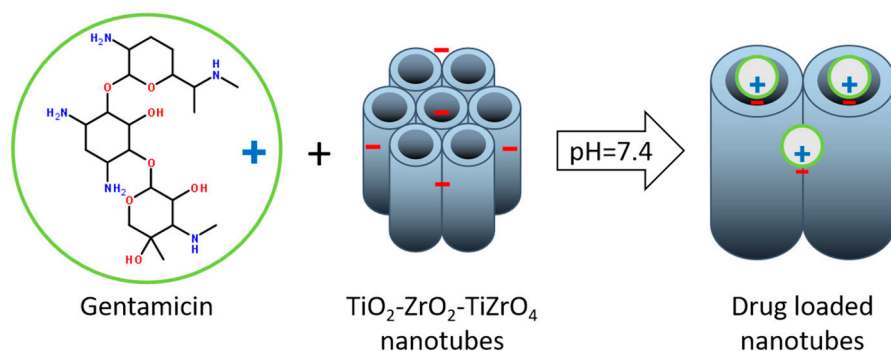


**Figure 5.** Schematic representation of gentamicin loading on  $\text{TiO}_2\text{-ZrO}_2\text{-ZrTiO}_4$  nanotubes via electrostatic interactions.

Another method of drug loading is the use of covalent anchoring of cationic antimicrobial agents to Ti alloy surfaces using a silane chemical-linker.

Song et al. [99] were among the first to study light-induced drug release from  $\text{TiO}_2$  nanotubes.  $\text{TiO}_2$  nanotubes were coated with (3-aminopropyl)triethoxysilane (APTES)—a siloxane linker loaded with horseradish peroxidase, which catalyzes the oxidation of various organic substrates—and capped with octadecylphosphonic acid.

Through this method, our group linked cysteine on Ti50Zr [37]. The cysteine sulfhydryl group is easily oxidized, giving some interesting properties. Cysteine has anti-inflammatory effects in human coronary arterial endothelial cells and is an excellent bacterial inhibitor [100]. Cysteine coated TiZr surfaces led to bacterial inhibitions as high as 56.74 % for *S. aureus* and 63.94% for *E. coli*, whereas the inhibition rates of polished Ti50Zr were 27.39 % for *S. aureus* and 29.15% for *E. coli*.

The inhibition rate is usually calculated by the following equation (Equation (5)):

$$I\% = \frac{(C_{24} - C_0) - (T_{24} - T_0)}{(C_{24} - C_0)} \times 100 \quad (5)$$

where  $I\%$  is the growth inhibition index,  $C_0$  is the blank-corrected optical density of the positive control at time 0,  $C_{24}$  is the blank-corrected optical density of the positive control after 24 h,  $T_0$  is the blank-corrected optical density of infected media in the presence of test samples, and  $T_{24}$  is the blank-corrected optical density of infected media in the presence of test samples at 24 h [41].

## 5. Conclusions

Based on the existing data, we can conclude that the biocompatibility of Ti50Zr is comparable to that of Roxolid and superior to that of cp-Ti. From an electrochemical testing perspective, Ti50Zr had the best corrosion resistance and stability compared to either pure Ti, pure Zr, or alloys with different Ti-Zr ratios. The superior mechanical properties of Ti50Zr make this alloy a better suited material for small dental implants. The  $\alpha$  structure of this alloy permits various surface treatments that enhance cell attachment and osseointegration. Depending on the purpose for which it is used, the surface of Ti50Zr can be tailored with relative ease to accommodate a wide range of structures, ranging from compact oxide to nano- and micropores, to more intricate structures such as nanotubes, nanochannels, and nanowires, an ability which is preserved from pure Ti. However, the same structures are harder to obtain with pure Zr. Drug loading and release from Ti50Zr is not well investigated and more extensive studies need to be done for this material, combining the excellent biocompatibility, electrochemical, and mechanical properties of this material with the benefits of targeted drug release. The investigations focused on biomedical applications of TiZr need to be continued to over a longer time period in order to validate its use in implants. Other industrial uses, such as for automotive purposes, solar cells, water splitting, or catalysts, may benefit from extensive research performed on Ti50Zr.

**Author Contributions:** Conceptualization, I.D.; investigation, D.I., C.P., and I.D.; data curation, D.I., C.P., and I.D.; writing—original draft preparation, D.I., C.P., A.B.S., and I.D.; writing—review and editing, A.B.S. and I.D.; visualization, A.B.S.; supervision, I.D. All authors have read and agreed to the published version of the manuscript.

**Acknowledgments:** The work has been supported by the Operational Program Human Capital of the Ministry of European Funds through the Financial Agreement 51668/09.07.2019, SMIS code 124705.

**Conflicts of Interest:** The authors declare no conflict of interest.

## References

- Zhang, L.C.; Chen, L.Y. A review on biomedical titanium alloys: Recent progress and prospect. *Adv. Eng. Mater.* **2019**, *21*, 1801215. [[CrossRef](#)]
- Daniela, I.; Man, I.; Demetrescu, I. The behaviour of electrochemical deposition of phosphate coating on CoCr bio alloys. *Key. Eng. Mater.* **2007**, 330–332, 545–548. [[CrossRef](#)]
- Hanawa, T. Zirconia versus titanium in dentistry: A review. *Dent. Mater. J* **2019**, *39*, 24–36. [[CrossRef](#)] [[PubMed](#)]
- Smeets, R.; Henningsen, A.; Jung, O.; Heiland, M.; Hammächer, C.; Stein, J.M. Definition, etiology, prevention and treatment of peri-implantitis—a review. *Head Face Med.* **2014**, *10*, 34. [[CrossRef](#)] [[PubMed](#)]
- Linetskiy, I.; Demenko, V.; Linetska, L.; Yefremov, O. Impact of annual bone loss and different bone quality on dental implant success—A finite element study. *Comput. Biol. Med.* **2017**, *91*, 318–325. [[CrossRef](#)] [[PubMed](#)]
- Bunoiu, I.; Andrei, M.; Scheau, C.; Manole, C.C.; Stoian, A.B.; Cioranu, V.; Didilescu, A. Electrochemical behavior of rejected dental implants in peri-implantitis. *Coatings* **2020**, *10*, 209. [[CrossRef](#)]
- Popa, M.; Vasilescu, E.; Drob, P.; Demetrescu, I.; Popescu, B.; Ionescu, D.; Vasilescu, C. In vitro assessment and monitoring of the implant titanium materials—Physiological environment interactions. *Mater. Corros.* **2003**, *54*, 215–221. [[CrossRef](#)]
- Osman, R.B.; Swain, M.V. A Critical Review of Dental Implant Materials with an Emphasis on Titanium versus Zirconia. *Materials* **2015**, *8*, 932–958. [[CrossRef](#)]
- Liu, X.; Chen, S.; Tsoi, J.K.H.; Matinlinna, J.P. Binary titanium alloys as dental implant materials—a review. *Regen. Biomater.* **2017**, *4*, 315–323. [[CrossRef](#)]
- Fisher, D.J. Additive Manufacturing of Metals. *Mater. Res. Found.* **2020**, *64*, 97–120. [[CrossRef](#)]
- Le Guéhennec, L.; Soueidan, A.; Layrolle, P.; Amouriq, Y. Surface treatments of titanium dental implants for rapid osseointegration. *Dent. Mater.* **2007**, *23*, 844–854. [[CrossRef](#)]
- Standard Specification for Wrought Titanium 6Al 4V ELI Alloy for Surgical Implants*; ASTM Designation F136-82; ASTM: Philadelphia, PA, USA, 1994; pp. 19–20.
- Okazaki, Y.; Gotoh, E.; Manabe, T.; Kobayashi, K. Comparison of metal concentrations in rat tibia tissues with various metallic implants. *Biomaterials* **2004**, *25*, 5913–5920. [[CrossRef](#)] [[PubMed](#)]

14. *Standard Specification for Wrought Titanium 6Al 7Nb Alloy for Surgical Implants*; ASTM Designation F1295-92; ASTM: Philadelphia, PA, USA, 1994; pp. 687–689.
15. Kim, K.T.; Eo, M.Y.; Nguyen, T.T.H.; Kim, S.M. General review of titanium toxicity. *Int. J. Implant Dent.* **2019**, *5*, 10. [[CrossRef](#)]
16. Bernhard, N.; Berner, S.; de Wild, M.; Wieland, M. The binary TiZr Alloy—A newly developed Ti alloy for the use in dental implants. *Forum. Implantol.* **2009**, *5*, 30–39.
17. Jimbo, R.; Naito, Y.; Galli, S.; Berner, S.; Dard, M.; Wennerberg, A. Biomechanical and histomorphometrical evaluation of TiZr alloy implants: An in vivo study in the rabbit. *Clin. Implant Dent. Relat. Res.* **2015**, *17*, 670. [[CrossRef](#)] [[PubMed](#)]
18. Grandin, H.M.; Berner, S.; Dard, M. A review of titanium zirconium (TiZr) alloys for use in endosseous dental implants. *Materials* **2012**, *5*, 1348–1360. [[CrossRef](#)]
19. Gottlow, J.; Dard, M.; Kjellson, F.; Obrecht, M.; Sennerby, L. Evaluation of a new titanium-zirconium dental implant: A biomechanical and histological comparative study in the mini pig. *Clin. Implant Dent. Relat. Res.* **2012**, *14*, 538–545. [[CrossRef](#)]
20. Wang, B.; Ruan, W.; Liu, J.; Zhang, T.; Hailin, Y.; Ruan, J. Microstructure mechanical properties, and preliminary biocompatibility evaluation of binary Ti–Zr alloys for dental application. *J. Biomater. Appl.* **2019**, *33*, 766–775. [[CrossRef](#)]
21. Gottlow, J. (Ed.) *Preclinical Data Presented at the 23rd Annual Meeting of the Academy of Osseointegration (AO)*; Straumann Holding AG: Boston, MA, USA; Basel, Switzerland, 2008; Available online: [www.straumann.com](http://www.straumann.com) (accessed on 20 April 2020).
22. Araki, H.; Nakano, T.; Ono, S.; Yatani, H. Three dimensional finite element analysis of extra short implant focusing on implant designs and materials. *Int. J. Implant Dent* **2020**, *29*, 5. [[CrossRef](#)] [[PubMed](#)]
23. Stoian, A.B.; Vardaki, M.; Ionita, D.; Enachescu, M.; Brancoveanu, O.; Demetrescu, I. Nanopores and nanotubes ceramic oxides elaborated on titanium alloy with zirconium by changing anodization by changing anodization potentials. *Ceram. Int.* **2018**, *44*, 7026–7033. [[CrossRef](#)]
24. Iegami, C.M.; Uehara, P.N.; Sesma, N.; Pannuti, C.M.; Tortamano Neto, P.; Mukai, M.K. Survival rate of titanium-zirconium narrow diameter dental implants versus commercially pure diameter dental implants versus commercially pure titanium diameter dental implants. *Clin. Implant Dent. Relat. Res.* **2017**, *19*, 1015–1022. [[CrossRef](#)] [[PubMed](#)]
25. Habazaki, H.; Uozumi, M.; Konno, H.; Shimizu, K.; Nagata, S.; Asami, K.; Matsumoto, K.; Takayama, K.; Oda, Y.; Skeldon, P.; et al. Influences of structure and composition on growth of anodic oxide films on TiZr alloys. *Electrochim. Acta* **2003**, *48*, 3257–3266. [[CrossRef](#)]
26. Akimoto, T.; Ueno, T.; Tsutsumi, Y.; Doi, H.; Hanawa, T.; Wakabayashi, N. Evaluation of corrosion resistance of implant-use Ti–Zr binary alloys with a range of compositions. *J. Biomed. Mater. Res. B* **2018**, *106B*, 73–79. [[CrossRef](#)] [[PubMed](#)]
27. Cui, W.; Liu, Y. Fatigue behavior of Ti50Zr alloy for dental implant application. *J Alloys Compd.* **2019**, *793*, 212–219. [[CrossRef](#)]
28. Mareci, D.; Bolat, G.; Chelariu, R.; Sutiman, D.; Munteanu, C. The estimation of corrosion behaviour of ZrTi binary alloys for dental applications using electrochemical techniques. *Mater. Chem. Phys.* **2013**, *141*, 362–369. [[CrossRef](#)]
29. Ion, R.; Stoian, A.B.; Dumitriu, C.; Grigorescu, S.; Mazare, A.; Cimpean, A.; Demetrescu, I.; Schmuki, P. Nanochannels formed on TiZr alloy improve biological response. *Acta Biomater.* **2015**, *24*, 370–377. [[CrossRef](#)] [[PubMed](#)]
30. Ion, R.; Mazare, A.; Dumitriu, C.; Pirvu, C.; Schmuki, P.; Cimpean, A. Nanochannelar topography positively modulates osteoblast differentiation and inhibits osteoclastogenesis. *Coatings* **2018**, *8*, 294. [[CrossRef](#)]
31. Stoian, A.B.; Surdu-Bob, C.; Anghel, A.; Ionita, D.; Demetrescu, I. Investigation of High Voltage Anodic Plasma (HVAP) Ag-DLC coatings on Ti50Zr with different Ag amounts. *Coatings* **2019**, *9*, 792. [[CrossRef](#)]
32. Gulec, F.; Sher, F.; Karaduman, A. Catalytic performance of Cu- and Zr-modified beta zeolite catalysts in the methylation of 2-methylnaphthalene. *Pet. Sci.* **2019**, *16*, 161–172. [[CrossRef](#)]
33. Zarren, G.; Nisar, B.; Sher, F. Synthesis of anthraquinone-based electroactive polymers: A critical review. *Mater. Today Sust.* **2019**, *5*, 100019. [[CrossRef](#)]
34. Navarro Amador, R.; Carboni, M.; Meyer, D. Photosensitive titanium and zirconium Metal Organic Frameworks: Current research and future possibilities. *Mater. Lett.* **2016**, *166*, 327–338. [[CrossRef](#)]

35. Liu, Q.; Wang, J. Dye-sensitized solar cells based on surficial TiO<sub>2</sub> modification. *Sol. Energy* **2019**, *184*, 454–465. [[CrossRef](#)]
36. Vardaki, M.; Mohajernia, S.; Pantazi, A.; Nica, I.C.; Enachescu, M.; Mazare, A.; Demetrescu, I.; Schmuki, P. Post treatments effect on TiZr nanostructures fabricated via anodizing. *J. Mater. Res. Technol.* **2019**, *8*, 5802–5812. [[CrossRef](#)]
37. Ho, W.F.; Chen, W.K.; Wu, S.C.; Hsu, H.C. Structure, mechanical properties, and grindability of dental Ti-Zr alloys. *J. Mater. Sci. Mater. Med.* **2008**, *19*, 3179. [[CrossRef](#)] [[PubMed](#)]
38. Pantazi, A.; Vardaki, M.; Mihai, G.; Ionita, D.; Stoian, A.B.; Enachescu, M.; Demetrescu, I. Understanding surface and interface properties of modified Ti50Zr with nanotubes. *Appl. Surf. Sci.* **2020**, *506*, 144661. [[CrossRef](#)]
39. Manole, C.C.; Dinischiotu, A.; Nica, I.C.; Demetrescu, I.; Pirvu, C. Influence of electrospun TiO<sub>2</sub> nanowires on corrosion resistance and cell response of Ti50Zr alloy. *Mater. Corros.* **2018**, *69*, 1609–1619. [[CrossRef](#)]
40. Stoian, A.B.; Demetrescu, I.; Ionita, D. Nanotubes and nano pores with chitosan construct on TiZr serving as drug reservoir. *Colloids Surf. B Biointerfaces* **2020**, *185*, 110535. [[CrossRef](#)]
41. Demetrescu, I.; Dumitriu, C.; Totea, G.; Nica, I.C.; Dinischiotu, A.; Ionita, D. Zwitterionic cysteine drug coating influence in functionalization of implantable Ti50Zr Alloy for antibacterial, biocompatibility and stability properties. *Pharmaceutics* **2018**, *10*, 220. [[CrossRef](#)]
42. Vardaki, M.; Ionita, D.; Stoian, A.B.; Demetrescu, I. Increasing corrosion resistance of a ZrTi alloy with a bioinspired coating with low porosity. *Mater. Corros.* **2017**, *68*, 988–994. [[CrossRef](#)]
43. Bolat, G.; Izquierdo, J.; Santana, J.; Mareci, D.; Souto, R.M. Electrochemical characterization of ZrTi alloys for biomedical applications. *Electrochim. Acta* **2013**, *88*, 447–456. [[CrossRef](#)]
44. Kim, W.G.; Choe, H.C.; Ko, Y.M.; Brantley, W.A. Nanotube morphology changes for Ti-Zr alloys as Zr content increases. *Thin Solid Films* **2009**, *517*, 5033–5037. [[CrossRef](#)]
45. Calderon Moreno, J.M.; Popa, M.; Ivanescu, S.; Vasilescu, C.; Drob, S.I.; Neacsu, E.I.; Popa, M.V. Microstructure, mechanical properties, and corrosion resistance of Ti-20Zr alloy in undoped and NaF doped artificial saliva. *Met. Mater. Int.* **2014**, *20*, 177–187. [[CrossRef](#)]
46. Zatkaličkov, V.; Palcek, P.; Markovicova, L.; Chalupov, M. Analysis of fractured screw shaped Ti6Al4V dental implant. *Mater. Today: Proc.* **2016**, *3*, 1216–1219. [[CrossRef](#)]
47. Croitoru, S.M.; Popovici, I.A. R&D on dental implants breakage. *Appl. Surf. Sci.* **2017**, *417*, 262–268. [[CrossRef](#)]
48. Barbosa, C.; Nascimento, J.L.; Centeno, R.O.; Caminha, I.M.V.; Abud, I.C. Failure analysis of titanium-based dental implant. *J. Fail. Anal. Prev.* **2010**, *10*, 138–142. [[CrossRef](#)]
49. Hernandez-Rodriguez, M.A.L.; Contreras-Hernandez, G.R.; Juarez-Hernandez, A.; Beltran-Ramirez, B.; Garcia-Sanchez, E. Failure analysis in a dental implant. *Eng. Fail. Anal.* **2015**, *57*, 236–242. [[CrossRef](#)]
50. International Organization for Standardization (ISO). *Dentistry-Implants-Dynamic Loading Test for Endosseous Dental Implants*; ISO 14801:2016; ISO: Geneva, Switzerland, 2016.
51. Sista, S.; Wen, C.; Hodgson, P.D.; Pande, G. The influence of surface energy of titanium-zirconium alloy on osteoblast cell functions in vitro. *J. Biomed. Mater. Res. A* **2011**, *97a*, 27. [[CrossRef](#)]
52. Prando, D.; Brenna, A.; Diamanti, M.V.; Beretta, S.; Bolzoni, F.; Ormellese, M.; Pedefferri, P. Corrosion of titanium: Part 1: Aggressive environments and main forms of degradation. *J. Appl. Biomater. Func.* **2017**, *15*, E291–E302. [[CrossRef](#)]
53. Zielinski, A.; Sobieszczyk, S. Corrosion of Titanium biomaterials, mechanisms, effects and modelisation. *Corros. Rev.* **2008**, *26*, 1–22. [[CrossRef](#)]
54. Zhang, Y.M.; Wang, Q.T.; Zhao, Y.M.; Guo, T.W.; Li, Z.C.; Hornez, J.C.; Hildebrand, H.F.; Tralsnel, M. Electrochemical Behavior of Titanium Alloys under Biological Conditions. *Rare Metal Mat. Eng.* **2004**, *33*, 19–22.
55. Siddiqui, D.A.; Guida, L.; Sridhar, S.; Valderrama, P.; Wilson, T.G.; Rodrigues, D.C. Evaluation of oral microbial corrosion on the surface degradation of dental implant materials. *J. Periodontol.* **2019**, *90*, 72–81. [[CrossRef](#)] [[PubMed](#)]
56. Dumitriu, C.; Popescu, S.; Ungureanu, C.; Pirvu, C. Antibacterial efficiencies of TiO<sub>2</sub> nanostructured layers prepared in organic viscous electrolytes. *Appl. Surf. Sci.* **2015**, *341*, 157–165. [[CrossRef](#)]
57. Mindroiu, M.; Pirvu, C.; Galateanu, B.; Demetrescu, I. Corrosion behaviour and cell viability of untreated and laser treated Ti6Al7Nb alloys. *Rev. Chim. –Buchar.* **2014**, *65*, 328–334.

58. Pirvu, C.; Demetrescu, I.; Drob, P.; Vasilescu, E.; Ivanescu, S.; Mindroiu, M.; Vasilescu, C.; Drob, S.I. Corrosion behaviour of a new Ti-6Al-2Nb-1Ta alloy in various solutions. *Mater. Corros.* **2011**, *62*, 948–955. [[CrossRef](#)]
59. Demetrescu, I.; Pirvu, C.; Mitran, V. Effect of nano-topographical features of Ti/TiO<sub>2</sub> electrode surface on cell response and electrochemical stability in artificial saliva. *Bioelectrochemistry* **2010**, *79*, 122–129. [[CrossRef](#)] [[PubMed](#)]
60. Demetrescu, I.; Ionita, D.; Pirvu, C.; Portan, D. Present and future trends in TiO<sub>2</sub> nanotubes elaboration, characterization and potential applications. *Mol. Cryst. Liq. Cryst.* **2010**, *521*, 195–203. [[CrossRef](#)]
61. Manole, C.C.; Pirvu, C.; Demetrescu, I. Evaluation of TiO<sub>2</sub> nanotubes changes after ultrasonication treatment. *Mol. Cryst. Liq. Cryst.* **2010**, *521*, 84–92. [[CrossRef](#)]
62. Manole, C.C.; Pirvu, C.; Demetrescu, I. TiO<sub>2</sub>: From nanotubes to nanopores by changing the anodizing voltage in fluoride-glycerol electrolyte. *Key. Eng. Mater.* **2009**, *415*, 5–8. [[CrossRef](#)]
63. Man, I.; Pirvu, C.; Demetrescu, I. Enhancing titanium stability in Fusayama saliva using electrochemical elaboration of TiO<sub>2</sub> nanotubes. *Rev. Chim. -Buchar.* **2008**, *59*, 615–617. [[CrossRef](#)]
64. Halley, I.; Ciosmak, D.; Lallemand, M.; Claude, J.M. Oxydation des alliages TiZr sous air et sous oxygène. III: Particularités morphologiques de l'interface substrat/oxyde de l'alliage Ti<sub>52</sub>Zr<sub>48</sub>. *J. Alloy Compd.* **1994**, *215*, 35–44. [[CrossRef](#)]
65. Halleydemoulin, I.; Ciosmak, D.; Lallemand, M. Oxydation des alliages TiZr sous air et sous oxygène II. Rôle de la composition des alliages sur l'évolution cinétique et morphologique du titane au zirconium. *J. Alloy Compd.* **1994**, *204*, 133–143. [[CrossRef](#)]
66. Wen, C.E.; Yamada, Y.; Hodgson, P.D. Fabrication of novel TiZr alloy foams for biomedical applications. *Mater. Sci. Eng. C* **2006**, *26*, 1439–1444. [[CrossRef](#)]
67. Chen, X.B.; Nouri, A.; Hodgson, P.D.; Wen, C.E. Surface modification of TiZr alloy for biomedical application. *Adv. Mater. Res.* **2007**, *15*, 89–94. [[CrossRef](#)]
68. Lu, J.; Zhang, Y.; Huo, W.; Zhang, W.; Zhao, Y.; Zhang, Y. Electrochemical corrosion characteristics and biocompatibility of nanostructured titanium for implants. *Appl. Surf. Sci.* **2018**, *434*, 63–72. [[CrossRef](#)]
69. Chen, X.B.; Nouri, A.; Li, Y.C.; Lin, J.G.; Hodgson, P.D.; Wen, C.E. Effect of surface roughness of Ti, Zr, and TiZr on apatite precipitation from simulated body fluid. *Biotechnol. Bioeng.* **2008**, *101*, 378–387. [[CrossRef](#)]
70. Wen, C.E.; Xu, W.; Hu, W.Y.; Hodgson, P.D. Hydroxiapatite /titania solgel coatings on titanium zirconia alloys for biomedical applications. *Acta Biomater.* **2007**, *3*, 403–410. [[CrossRef](#)]
71. Vardaki, M.; Prodana, M.; Stoian, A.B.; Ionita, D. Corrosion and bioactivity of a bioinspired coating on TiZr alloys. *Sci. Bull. Univ. Politeh. Buchar.* **2018**, *80*, 209–217.
72. Ma, J.; Wong, H.; Kong, L.B.; Peng, K.W. Biomimetic processing nanocrystalline apatite coatings on titanium zirconium alloy. *Nanotechnology* **2003**, *14*, 619–623. [[CrossRef](#)]
73. Minagar, S.; Berndt, C.; Gengenbach, T.; Wen, C. Fabrication and characterization of TiO<sub>2</sub>-ZrO<sub>2</sub>-ZrTiO<sub>4</sub> nanotubes on TiZr alloy manufactured via anodization. *J. Mater. Chem. B* **2014**, *2*, 71–83. [[CrossRef](#)]
74. Minagar, S.; Li, Y.; Berndt, C.C.; Wen, C. The influence of Titania-Zirconia-Zirconium titanate nanotube characteristics on osteoblast cell adhesion. *Acta Biomater.* **2014**, *12*, 281–289. [[CrossRef](#)]
75. Yun, K.D.; Yang, Y.; Lim, H.P.; Oh, G.J.; Koh, J.T.; Bae, I.H.; Kim, J.; Lee, K.M.; Park, S.W. Effect of nanotubular-micro-roughened titanium surface on cell response in vitro and osseointegration in vivo. *Mater. Sci. Eng. C* **2010**, *30*, 27–33. [[CrossRef](#)]
76. Sista, S.; Nouri, A.; Li, Y.; Wen, C.; Hodgson, P.D.; Pande, G. Cell biological responses of osteoblasts on anodized nanotubular surface of a titanium—zirconium alloy. *J. Biomed. Mater. Res. A* **2013**, *101*, 3416–3430. [[CrossRef](#)] [[PubMed](#)]
77. Jha, H.; Hahn, R.; Schmuki, P. Ultrafast oxide nanotube formation on TiNb, TiZr and TiTa alloys by rapid breakdown anodization. *Electrochim. Acta* **2010**, *55*, 8883–8887. [[CrossRef](#)]
78. Grigorescu, S.; Pruna, V.; Titorencu, I.; Jinga, V.; Mazare, A.; Schmuki, P.; Demetrescu, I. The two step nano tube formation on TiZr as scaffolds for cell growth. *Bioelectrochem* **2014**, *98*, 39–45. [[CrossRef](#)]
79. Grigorescu, S.; Ungureanu, C.; Kirchgorg, R.; Schmuki, P.; Demetrescu, I. Various sized nanotubes on TiZr for antibacterial surfaces. *Appl. Surf. Sci.* **2013**, *270*, 190–196. [[CrossRef](#)]
80. Murphy, M.; Walczak, M.S.; Thomas, A.G.; Silikas, N.; Berner, S.; Lindsay, R. Toward optimizing dental implant performance: Surface characterization of Ti and TiZr implant materials. *Dent. Mater.* **2017**, *33*, 43–53. [[CrossRef](#)]

81. Cordeiro, M.; Pantaroto, H.N.; Paschoaleto, E.M.; Rangel, E.C.; da Cruz, N.C.; Sukotjo, C.; Barao, V.A.R. Synthesis of biofunctional coating for a TiZr alloy: Surface, electrochemical, and biological characterizations. *Appl. Surf. Sci.* **2018**, *452*, 268–278. [[CrossRef](#)]
82. Kaluderovic, M.R.; Krajnovic, T.; Maksimovic-Ivanic, D.; Graf, H.L.; Mijatovic, S. Ti-SLActive and TiZr-SLActive dental implant surfaces promote fast osteoblast differentiation. *Coatings* **2017**, *7*, 102. [[CrossRef](#)]
83. Yin, L.H.; Chang, Y.R.; You, Y.H.; Liu, C.; Li, J.; Lai, H.C. Biological responses of human bone mesenchymal stem cells to Ti and TiZr implant materials. *Clin. Implant Dent. R* **2019**, *21*, 550–564. [[CrossRef](#)]
84. Roy, S.; Berger, S.; Schmuki, P. TiO<sub>2</sub> nanotubes: Synthesis and applications. *Agew. Chem. Int. Ed.* **2011**, *50*, 2904–2939. [[CrossRef](#)]
85. Macak, J.; Hildebrand, H.; Marten-Jahns, U.; Schmuki, P. Mechanistic aspects and growth of large diameter self-organized TiO<sub>2</sub> nanotubes. *J. Electroanal. Chem.* **2008**, *621*, 254–266. [[CrossRef](#)]
86. Gulati, K.; Kogawa, M.; Prideaux, M.; Findlay, D.M.; Atkins, G.J.; Losic, D. Drug-releasing nanoengineered titanium implants: Therapeutics efficacy in 3D cell culture model, controlled release and stability. *Mater. Sci. Eng. C* **2016**, *69*, 831–840. [[CrossRef](#)] [[PubMed](#)]
87. Gulati, K.; Maher, S.; Chandrasekaran, S.; Findlay, D.M.; Losic, D. Conversion of titania (TiO<sub>2</sub>) in conductive titanium (Ti) nanotube arrays for combined drug-delivery and electrical simulation therapy. *J. Mater. Chem. B* **2015**, *14*, 371–375. [[CrossRef](#)]
88. Higuchi, T. Mechanism of sustained—action medication. Theoretical analysis of rate of release of solid drugs dispersed in solid matrices. *J. Pharm. Sci.* **1963**, *52*, 1145–1149. [[CrossRef](#)] [[PubMed](#)]
89. Korsmeyer, R.W.; Gurny, R.; Doelker, E.; Buri, P.; Peppas, N.A. Mechanisms of solute release from porous hydrophilic polymers. *Int. J. Pharm.* **1983**, *15*, 25–35. [[CrossRef](#)]
90. Peppas, N.A.; Sahlin, J.J. A simple equation for the description of solute release. III. Coupling of diffusion and relaxation. *Int. J. Pharm.* **1989**, *57*, 169–172. [[CrossRef](#)]
91. Lindner, W.D.; Lippold, B.C. Drug release from hydrocolloid embeddings with high or low susceptibility to hydrodynamic stress. *Pharm. Res.* **1995**, *12*, 1781–1785. [[CrossRef](#)]
92. Popat, K.; Eltgroth, M.; LaTempa, T.; Grimes, C.; Desai, T. Titania nanotubes: A novel platform for drug-eluting coatings for medical implants? *Small* **2007**, *3*, 1878–1881. [[CrossRef](#)]
93. Peng, L.; Mendelsohn, A.; LaTempa, T.; Yoriya, S.; Grimes, C.; Desai, T. Long-term small molecule and protein elution from TiO<sub>2</sub> nanotubes. *Nano Lett.* **2009**, *9*, 1932–1936. [[CrossRef](#)]
94. Nemati, S.H.; Hadjizadeh, A. Gentamicin-eluting titanium dioxide nanotubes grown on the ultrafine-grained titanium. *AAPS Pharm. Sci. Tech.* **2017**, *18*, 2180–2187. [[CrossRef](#)]
95. Aw, M.; Gulati, K.; Losic, D. Controlling drug release from titania nanotube arrays using polymer nanocarriers and biopolymer coating. *J. Biomater. Nanobiotechnol.* **2011**, *2*, 477–484. [[CrossRef](#)]
96. Kumeria, T.; Mon, H.; Aw, M.S.; Gulati, K.; Santos, A.; Griesser, H.J.; Losic, D. Advanced biopolymer-coated drug-releasing titania nanotubes (TNTs) implants with simultaneously enhanced osteoblast adhesion and antibacterial properties. *Colloid. Surf. B: Biointerfaces* **2015**, *1*, 255–263. [[CrossRef](#)]
97. Vasilev, K.; Cook, J.; Griesser, H.J. Antibacterial surfaces for biomedical devices. *Expert Rev. Med. Devices* **2009**, *6*, 553–567. [[CrossRef](#)] [[PubMed](#)]
98. Hetrick, E.M.; Schoenfisch, M.H. Reducing implant-related infections: Active release strategies. *Chem. Soc. Rev.* **2006**, *35*, 780–789. [[CrossRef](#)] [[PubMed](#)]
99. Song, Y.Y.; Schmidt-Stein, F.; Bauer, S.; Schmuki, P. Amphiphilic TiO<sub>2</sub> nanotube arrays: An actively controllable drug delivery system. *J. Am. Chem. Soc.* **2009**, *131*, 4230–4232. [[CrossRef](#)]
100. Hasegawa, S.; Ichiyama, T.; Sonaka, I.; Ohsaki, A.; Okada, S.; Wakiguchi, H.; Kudo, K.; Kittaka, S.; Hara, M.; Furukawa, S. Cysteine, Histidine and Glycine exhibit anti-inflammatory effects in human coronary arterial endothelial cells. *Clin. Exp. Immunol.* **2012**, *167*, 269–274. [[CrossRef](#)]

